

Theory of the magnetic phase diagram of LiHoF₄

P. B. Chakraborty,^{1,2} P. Henelius,³ H. Kjønsberg,⁴ A. W. Sandvik,^{5,6} and S. M. Girvin²

¹Department of Physics, Indiana University, Bloomington, Indiana 47405, USA

²Department of Physics, Yale University, P. O. Box 208120, New Haven, Connecticut 06520-8120, USA

³Condensed Matter Theory, Royal Institute of Technology, SE-106 91 Stockholm, Sweden

⁴Telenor R & D, Snarøyveien 30, Fornebu 1331, Norway

⁵Department of Physics, Boston University, 590 Commonwealth Avenue, Boston, Massachusetts 02215, USA

⁶Department of Physics, Åbo Akademi University, Porhansgatan 3, FIN-20500, Åbo, Finland

(Received 16 April 2004; revised manuscript received 6 August 2004; published 21 October 2004)

The properties of LiHoF₄ are believed to be well described by a long-range dipolar Ising model. We go beyond mean-field theory and calculate the phase diagram of the Ising model in a transverse field using a quantum Monte Carlo method. The relevant Ising degrees of freedom are obtained using a nonperturbative projection onto the low-lying crystal-field eigenstates. We explicitly take the domain structure into account, and the strength of the near-neighbor exchange interaction is obtained as a fitting parameter. The on-site hyperfine interaction is approximately taken into account through a renormalization of the transverse applied magnetic field. Finally, we propose a spectroscopy experiment to precisely measure the most important parameter controlling the location of the phase boundary.

DOI: 10.1103/PhysRevB.70.144411

PACS number(s): 75.10.Jm, 75.40.Mg, 75.70.Ak, 75.30.Gw

I. INTRODUCTION

In the last decade, the rare-earth compound LiHoF₄ has been found to display an array of interesting magnetic phenomena. At high temperatures LiHoF₄ is a paramagnet, but there is a second-order transition to a ferromagnetic state at 1.53 K.¹ This Ising magnetic transition is driven by the weak magnetic dipole interaction, with a strength of order 1 K, and not the more usual Coulomb exchange interaction. The critical temperature can be lowered by application of a magnetic field transverse to the easy-axis direction of ferromagnetic ordering. The magnetic field introduces quantum fluctuations of the spins and beyond a critical value of ~ 4.9 T, destroys long-range ordering even at zero temperature. LiHoF₄ thus represents a model magnet for studying quantum phase transitions.² Since the rate of quantum tunneling between different spin configurations can be carefully controlled with the transverse magnetic field, this material constitutes a good testing ground for the efficiency of quantum annealing.³ By substituting the magnetic Ho³⁺ ions with nonmagnetic Y³⁺ ions, disorder can be introduced, and spin-glass behavior has been observed when the magnetic ions are sufficiently dilute.⁴ On further dilution the range of dynamic time scales displays a remarkable narrowing in what has been called the “antiglass” phase.⁵

The magnetic properties of LiHoF₄ originate in the Ho³⁺ ions. The ground state of the Ho³⁺ ion in the crystal field is a doublet, and the first excited state is ~ 11 K above the ground state. The crystal-field states of the Ho³⁺ ion are such that there are no matrix elements of the transverse angular momentum (J_x, J_y) within the ground-state doublet. Hence the transverse susceptibility vanishes (to lowest order in the applied field) giving rise to strong Ising anisotropy. Therefore LiHoF₄ in a transverse magnetic field, and at temperatures lower than ~ 11 K, is believed to be a very good realization of a dipolar Ising model

$$H = \frac{1}{2} \sum_{i \neq j} J \frac{r_{ij}^2 - 3z_{ij}^2}{r_{ij}^5} S_i^z S_j^z - h^x \sum_i S_i^x, \quad (1)$$

where J is the coupling constant, r_{ij} the interspin distance, and z_{ij} the component of the interspin distance along the Ising axis. The effective transverse field parameter h^x is a measure of the (higher order) mixing effects introduced by the physical transverse magnetic field. The summation is done over all Ho³⁺ ions, which sit on a tetragonal Bravais lattice with four Ho³⁺ ions per unit cell.⁴

The goal of the present study is to determine the quantitative phase diagram of pure LiHoF₄ from (quasi) first principles, starting from a crystal-field Hamiltonian that has been fit to spectroscopic data. Bitko *et al.*² successfully fit their phase diagram data using a mean-field theory with two free parameters, a transverse susceptibility $g_{\perp} \approx 0.74$ to replace the Landé g factor $g_L = 1.25$ which thus rescales the transverse field, and an effective dipole coupling strength J_0 which rescales the temperature. This calculation also did not take into account the domain structure of the ferromagnetic state. In another calculation, Rønnow *et al.*⁶ have recently used an RPA method to find the collective mode softening seen in their neutron scattering measurements and obtain an estimate of the phase diagram.

The advancements reported in the present study over earlier attempts are twofold. We develop an effective low-energy Hamiltonian (derived nonperturbatively by projection from the full 17 state crystal-field Hamiltonian) that acts on spin- $\frac{1}{2}$ Ising degrees of freedom, and we go beyond simple mean-field theory by using extensive quantum Monte Carlo simulations. An earlier classical Monte Carlo study found a critical temperature of 1.89 K by extrapolation from rather limited system sizes.⁷ However, they did not take into account a near-neighbor exchange interaction among the Ho³⁺ ions and the structure of domains observed in LiHoF₄. Yet

another Monte Carlo study finds a transition temperature of 1.51 K, but only by adjusting the strength of the dipolar interaction to reproduce the experimentally determined ground-state energy.⁸ Here we explicitly take the domain structure of LiHoF₄ into account and use a much improved method which vastly reduces finite-size corrections. We also use a recently introduced cluster algorithm.⁹ In this manner we can determine both the critical temperature and critical field of the effective Ising model with high precision. This precision is high enough that the (considerable) uncertainties in the crystal field parameters (described below) are now the limiting factors controlling uncertainties in the predicted phase diagram. We will propose a simple microwave spectroscopy experiment to eliminate these experimental uncertainties.

II. THE CRYSTAL FIELD HAMILTONIAN

A single Ho³⁺ ion in the crystal LiHoF₄ has a partially filled outermost shell $4f^{10}$, and the ground-state electronic configuration of the Ho³⁺ ion is 5I_8 as dictated by Hund's rules. The lowest excited electronic configuration of the ion 5I_7 lies approximately 7400 K above the ground-state configuration, as seen in spectroscopic experiments on LiHoF₄.¹⁰ In the range of temperatures of interest in this article, any configuration mixing of the ground configuration with the excited ones can thus be safely neglected. The configuration mixing due to the crystal field is also assumed to be small.

Considering only the spin-orbit interaction and the Hund's Rules, the ground-state configuration of the Ho³⁺ ion in LiHoF₄ will be $(2J+1)=17$ -fold degenerate. But the interaction of Ho³⁺ with the Li⁺ and F⁻ ions can be captured concisely in a crystal-field Hamiltonian (V_C) that lifts the degeneracy while taking into account the symmetry of the crystal. The LiHoF₄ crystal has S_4 symmetry, which partially splits the 17-fold degeneracy. In S_4 symmetry, the states of a configuration with an even number of electrons transform according to four one-dimensional representations, two of which are related by time-reversal symmetry. The ground state of the crystal-field Hamiltonian is thus a doublet, belonging to the two related representations mentioned above, giving rise to a non-Kramers degenerate ground state. The crystal-field Hamiltonian depends in a complicated way on the positions of the various ions inside a unit cell, but it turns out that one can express V_C in terms of the total angular momentum (\vec{J}) operators of the Ho³⁺ ions by using a set of Steven's equivalent operators and corresponding phenomenological constants called crystal-field parameters (CFP) which are determined by fitting to experimental spectroscopic and susceptibility data.^{10,11} (See the Appendix for details on the crystal-field Hamiltonian.)

Ising system at low temperatures. Diagonalizing V_C shows that the lowest excited state in the spectrum is a singlet, lying ~ 11 K above the ground state doublet. At temperatures much lower than this gap, only the ground-state doublet can be expected to be significantly populated, and the low-temperature physics can be captured by considering a two-state system. The two degenerate states (denoted by $|\alpha\rangle$ and

$|\beta\rangle$) can be chosen such that $\langle\alpha|J^x|\alpha\rangle=-\langle\beta|J^x|\beta\rangle$ and $\langle\alpha|J^z|\beta\rangle=0$. It turns out that the transverse angular momentum operators J^x and J^y have no nonzero matrix elements in the degenerate ground-state subspace. This is the source of the strong Ising anisotropy which causes the linear susceptibility to vanish in the transverse directions. We thus identify the two degenerate states as $|\uparrow\rangle$ and $|\downarrow\rangle$, and it can be expected that the low-temperature physics will be described by an effective Ising model with spin- $\frac{1}{2}$ degrees of freedom.

The S_4 symmetry of the crystal defines an easy axis for ferromagnetic ordering in the pure LiHoF₄ crystal.² In the absence of any externally applied magnetic field, the magnetic dipole interaction among the Ho³⁺ magnetic moments causes them to align along the c axis of the unit cell (the z direction in this analysis) below 1.53 K and the dipolar Ising model serves as an adequate effective model for the system.

The situation becomes more subtle when the crystal is subjected to an external magnetic field perpendicular to the abovementioned easy axis.² The magnetic moments couple to the transverse field through the Zeeman interaction. Restricted within the ground-state configuration $J=8$, the Wigner-Eckert theorem yields a Landé g factor $g_L=\frac{5}{4}$ and the Zeeman term in the Hamiltonian can be written as

$$H_Z = -g_L\mu_B\vec{B}\cdot\vec{J}, \quad (2)$$

with $\mu_B=0.6717$ K/T being the Bohr magneton and $\vec{B}=B_x\hat{e}_x$. Because the Zeeman term has no matrix elements within the two-dimensional subspace, it cannot flip a spin to first order in \vec{B} . Thus to see any effect of the transverse field one must resort to second-order perturbation theory. Denoting the singlet excited state at $\Delta=11$ K by $|\gamma\rangle$, one can expect to see an effect $\sim(g_L\mu_B)^2(B_x^2/\Delta)|\langle\gamma|J^x|\alpha,\beta\rangle|^2$ on the energies of the ground states. A naive application of degenerate second-order perturbation theory thus suggests that the effect of the transverse field should be proportional to B_x^2 .

This perturbation theory scenario breaks down in the quantum critical regime as can be seen in a comparison of the energies. If we assume that the magnetic moment is fully polarized in the transverse direction ($\langle J^y\rangle=J=8$) at the quantum critical point of $B_x^c=4.9$ T at $T=0$,² a simple estimate of the Zeeman energy is given by

$$E_Z = g_L\mu_B B_x^c \langle J^x \rangle = 32.91 \text{ K}, \quad (3)$$

significantly larger than Δ . This demonstrates that the mixing of the ground-state doublet with all the higher-lying states must be considered at large transverse fields and second-order perturbation theory is not sufficient to incorporate the effect of \vec{B} in the quantum critical regime. We describe below a nonperturbative scheme to capture this physics.

III. MAPPING TO THE ISING SYSTEM

The magnetic properties of LiHoF₄ are determined by three kinds of interactions: a long-range magnetic dipole interaction among the Ho³⁺ magnetic moments, a near-neighbor exchange interaction which we assume to be small and isotropic, and an isotropic hyperfine interaction between

the electronic and nuclear magnetic moments on the same site. Therefore, the complete Hamiltonian of a LiHoF₄ crystal in a transverse magnetic field can be written as

$$H = \sum_i V_C(\vec{J}_i) - g_L \mu_B \sum_i B_x J_i^x + \frac{1}{2} (g_L \mu_B)^2 \sum_{i \neq j} \mathcal{L}_{ij}^{\mu\nu} J_i^\mu J_j^\nu + \frac{1}{2} (g_L \mu_B)^2 \frac{J_{\text{ex}}}{a^3} \sum_{i,nn} \vec{J}_i \cdot \vec{J}_{nn} + A \sum_i (\vec{I}_i \cdot \vec{J}_i), \quad (4)$$

where $\mu, \nu = x, y, z$. $\mathcal{L}_{ij}^{\mu\nu}$ contains the position dependence of the magnetic dipole interaction so that

$$\mathcal{L}_{ij}^{\mu\nu} = \frac{\mathcal{D}^{\mu\nu} |\vec{r}_{ij}|^2 - 3(\vec{r}_{ij})^\mu (\vec{r}_{ij})^\nu}{|\vec{r}_{ij}|^5}. \quad (5)$$

J_{ex} is the dimensionless strength of the antiferromagnetic exchange interaction (whose strength is unknown at this point), NN signifies that the sum is to be carried out over nearest neighbors only and $a (=5.175 \text{ \AA})$ is the length of the unit cell in the x - y plane. A is the strength of the hyperfine interaction (0.039 K) and \vec{I}_i is the total angular momentum vector of the Ho nucleus at the i th site $I = \frac{7}{2}$.

To reduce the Hamiltonian that acts on a $(2J+1) \times (2I+1) = 136$ -dimensional Hilbert space to an effective Ising model with spin- $\frac{1}{2}$ degrees of freedom, we neglect the relatively weak hyperfine interaction in a first approximation. If $A=0$, the only relevant degrees of freedom are the electronic angular momenta \vec{J} and, for $J=8$, the single-site Hilbert space is 17-dimensional. The transverse field splits the degeneracy in the ground-state subspace and also mixes the 15 higher-lying crystal-field states with the two lowest states. The single-site Hamiltonian (neglecting the hyperfine interaction)

$$H_T = V_C(\vec{J}) - g_L \mu_B B_x J^x \quad (6)$$

is diagonalized numerically for all values of the transverse field. For a given B_x , let the two lowest states be denoted by $|\alpha(B_x)\rangle$ and $|\beta(B_x)\rangle$ and their energies be denoted by $E_\alpha(B_x)$ and $E_\beta(B_x)$. Then in a two-dimensional Hilbert space which is spanned by $|\alpha(B_x)\rangle$ and $|\beta(B_x)\rangle$ (identified as $|\rightarrow\rangle$ and $|\leftarrow\rangle$, respectively) H_T can be written as

$$H_T = E_{CM}(B_x) - \frac{1}{2} \Delta(B_x) \sigma^x, \quad (7)$$

where $E_{CM}(B_x) = \frac{1}{2} [E_\alpha(B_x) + E_\beta(B_x)]$ and $\Delta(B_x) = E_\beta(B_x) - E_\alpha(B_x)$. Thus we see that the energy difference between the degenerate states caused by the transverse field can already be interpreted as an effective magnetic field acting on spin- $\frac{1}{2}$

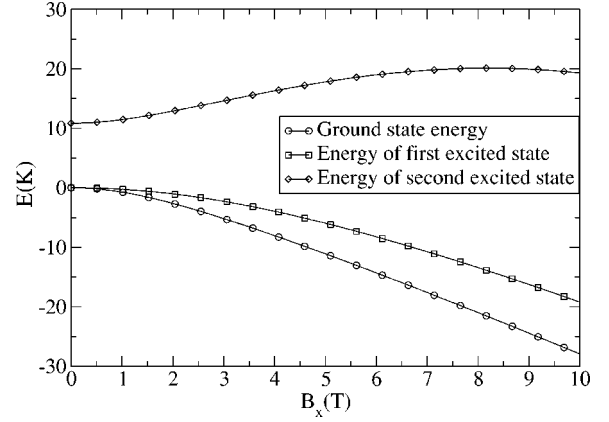


FIG. 1. Lifting of ground-state degeneracy by the transverse field.

degrees of freedom at each site. Figure 1 demonstrates how the transverse field continuously splits the degeneracy between the two ground states.

To generate the complete first-principles Hamiltonian in Eq. (4) in terms of the Ising spins, one must project the \vec{J} operators onto the two-dimensional subspace. Recognizing the fact that every two-dimensional Hermitian matrix can be uniquely expanded in terms of the two-dimensional unit matrix and the three Pauli matrices, we evaluate the matrix elements of the \vec{J} operators within the two-dimensional subspace for each value of the magnetic field and obtain their representations in terms of spin- $\frac{1}{2}$ operators. Every operator J^μ ($\mu = x, y, z$) can be written as

$$J^\mu = C_\mu + \sum_{\nu=x,y,z} C_{\mu\nu}(B_x) \sigma^\nu. \quad (8)$$

The Pauli matrices σ^ν requires the choice of a basis $|\uparrow\rangle$ and $|\downarrow\rangle$ in terms of the states $|\alpha\rangle$ and $|\beta\rangle$. We choose the basis vectors such that $|\uparrow\rangle = (1/\sqrt{2})[|\alpha\rangle + \exp(i\theta)|\beta\rangle]$ and $|\downarrow\rangle = (1/\sqrt{2})[|\alpha\rangle - \exp(i\theta)|\beta\rangle]$. The phase θ is chosen such that the matrix elements of the operator J^z are real. In this basis, we have

$$J_i^z = C_{zz} \sigma_i^z. \quad (9)$$

The operators J^x and J^y are also projected into this basis. Table I presents the values of the various parameters C_μ and $C_{\mu\nu}$, for $B_x = 4.9$ T, which is the experimentally observed critical transverse field in the limit of vanishing temperature.

We replace the \vec{J} operators by their corresponding representations in the two-dimensional basis in the Hamiltonian in Eq. (4). (The hyperfine interaction is neglected at this stage.)

TABLE I. The strengths of various coefficients $C_{\mu\nu}$ for $B_x = 4.9$ T.

C_z	0	C_x	3.12	C_y	0.01
C_{zx}	0	C_{xx}	0.60	C_{yx}	-0.09
C_{zy}	0	C_{xy}	0.01	C_{yy}	1.05
C_{zz}	5.14	C_{xz}	0	C_{yz}	0

This leads to an extremely complicated Hamiltonian that acts on the Ising subspace. The projection generates various new kinds of interactions among the effective Ising spins. For example, the term

$$H_{zx} = \frac{1}{2}(g_L\mu_B)^2 \sum_{i \neq j} \mathcal{L}_{ij}^{zx} J_i^z J_j^x$$

in Eq. (4) gives rise to a set of complicated interactions in the Ising subspace that are written as

$$\begin{aligned} H_{zx} &= \frac{1}{2}(g_L\mu_B)^2 \sum_{i \neq j} \mathcal{L}_{ij}^{zx} (C_{zz}\sigma_i^z) (C_x + C_{xx}\sigma_j^x + C_{xy}\sigma_j^y) \\ &= \frac{1}{2}(g_L\mu_B)^2 \sum_i \left(\sum_{j \neq 0} \mathcal{L}_{j0}^{zx} \right) C_{zz} C_x \sigma_i^z \\ &\quad + \frac{1}{2}(g_L\mu_B)^2 \sum_{i \neq j} \mathcal{L}_{ij}^{zx} C_{zz} C_{xx} \sigma_i^z \sigma_j^x \\ &\quad + \frac{1}{2}(g_L\mu_B)^2 \sum_{i \neq j} \mathcal{L}_{ij}^{zx} C_{zz} C_{xy} \sigma_i^z \sigma_j^y. \end{aligned} \quad (10)$$

In Eq. (10), the quantities C_{zz} , etc., depend on the transverse magnetic field B_x . The strength of the effective interactions generated by the Ising projection is determined not only by the parameters $C_{\mu\nu}$, but also by the parameters $\mathcal{L}_{ij}^{\alpha\beta}$, that depend on the interspin vector \vec{r}_{ij} . Thus we can compare the strengths of the various effective interactions, and we find that the largest effective interaction is $J_i^z J_j^z \propto (C_{zz})^2 \sigma_i^z \sigma_j^z$. This interaction is larger than the other interaction terms by two orders of magnitude for the entire range of magnetic fields in question (except for some constant terms that just serves to define a new zero of energy). Therefore, to an accuracy of $\sim 1\%$, the effective Ising model for LiHoF₄ can now be written as

$$\begin{aligned} H_{\text{Ising}} &= \sum_i E_{CM,i}(B_x) - \frac{1}{2}\Delta(B_x) \sum_i \sigma_i^x \\ &\quad + \frac{1}{2}(g_L\mu_B C_{zz})^2 \sum_{i \neq j} \mathcal{L}_{ij}^{zz} \sigma_i^z \sigma_j^z \\ &\quad + \frac{1}{2}(g_L\mu_B C_{zz})^2 \frac{J_{\text{ex}}}{a^3} \sum_{i,nn} \sigma_i^z \sigma_{nn}^z. \end{aligned} \quad (11)$$

The Ising Hamiltonian of Eq. (11) acts on effective spin- $\frac{1}{2}$ objects (“pseudospins”) located at the lattice sites of Ho³⁺ ions in the pure crystal LiHoF₄, and the interaction strengths and the effective transverse field depend on the physical transverse field B_x implicitly through the parameters C_{zz} and Δ . The parameter E_{CM} provides a B_x -dependent zero of energy and will be ignored for the purpose of computing the magnetic phase diagram.

IV. COMPUTING THE PHASE DIAGRAM

Equation (11) is a particular example of a general class of Hamiltonians in which the various terms in the Hamiltonian do not commute with each other, and in the interesting pa-

rameter regime around the quantum critical point, they are comparable in strength. Therefore, quantum fluctuations can become strong enough in the system to destroy long-range order even at $T=0$. An Ising model of spin- $\frac{1}{2}$ objects on a three dimensional lattice placed in a magnetic field transverse to the Ising direction is a very good prototype of such a Hamiltonian. We utilize Eq. (11) as a starting point to compute the phase diagram of LiHoF₄ in various ways, notably using mean-field theory and quantum Monte Carlo simulations. As a spin-off, we are able to calculate the strength of the exchange interaction J_{ex} . Finally, we compare our results with existing experimental data,² which were obtained from magnetic susceptibility measurements.

A. The effective Hamiltonian

An unusual feature of the Ising Hamiltonian in Eq. (11) is that the strength of the dipole interaction itself seems to depend explicitly on the strength of the physical transverse field through the parameter C_{zz} . Ordinarily, the interaction term in an Ising model is free of any dependence on external magnetic fields. The popular Hamiltonian governing the quantum Ising model is generically written as

$$H_{\text{gen}} = \frac{1}{2} \sum_{i \neq j} J_{ij} \sigma_i^z \sigma_j^z - h^x \sum_i \sigma_i^x, \quad (12)$$

where J_{ij} is the pairwise interaction term (dipole interaction, near-neighbor exchange,...) which usually depends on the difference in spatial positions of the spins, and h^x is the magnetic field that acts as the source of the quantum fluctuations. With some appropriate definitions, we are able to define an effective model H_{eff} that is of the same general form as Eq. (12).

The reduction to a two dimensional Hilbert space from a 17-dimensional Hilbert space gives rise to renormalized Landé g factor g_{\parallel} , defined as

$$g_{\parallel} = 2g_L \langle \alpha(B_x=0) | J^z | \alpha(B_x=0) \rangle = 13.8. \quad (13)$$

The factor $2g_L C_{zz}(B_x)$ can be interpreted as a renormalization of the individual magnetic moments due to the presence of the transverse magnetic field. To extract this renormalization factor, we define a dimensionless ratio $\epsilon(B_x)$ such that

$$\epsilon(B_x) = \frac{2g_L C_{zz}(B_x)}{g_{\parallel}}. \quad (14)$$

In the classical limit $B_x=0$, $\epsilon(B_x)=1$ by definition. This makes it possible to define an effective Hamiltonian H_{eff} , which is essentially identical to Eq. (12).

$$H_{\text{Ising}} = [\epsilon(B_x)]^2 H_{\text{eff}}, \quad (15)$$

where

$$\begin{aligned} H_{\text{eff}} &= \frac{1}{2} \sum_{i \neq j} \left(\frac{g_{\parallel} \mu_B}{2} \right)^2 \mathcal{L}_{ij}^{zz} \sigma_i^z \sigma_j^z + \frac{1}{2} \sum_{i,nn} \left(\frac{g_{\parallel} \mu_B}{2} \right)^2 \frac{J_{\text{ex}}}{a^3} \sigma_i^z \sigma_{nn}^z \\ &\quad - \frac{\Delta(B_x)}{2[\epsilon(B_x)]^2} \sum_i \sigma_i^x. \end{aligned} \quad (16)$$

We define every length in the system in units of a

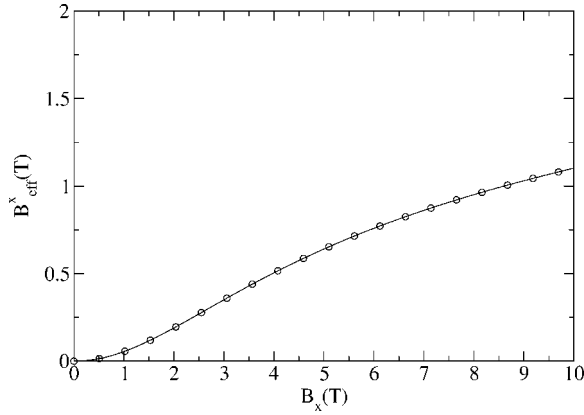


FIG. 2. The effective magnetic field.

$=5.175 \text{ \AA}$, such that $\tilde{r}_{ij}^\mu = r_{ij}^\mu/a$. Then the spatial dependence of the dipole interactions can be expressed in the terms of dimensionless quantities $L_{ij}^{\mu\nu}$, defined as $\mathcal{L}_{ij}^{\mu\nu} = L_{ij}^{\mu\nu}/a^3$. Replacing the constants in Eq. (16), we see that $(g_{\parallel}\mu_B/2)^2 1/a^3 = 0.214 \text{ K}$, and $(g_{\parallel}\mu_B/2) = 4.635 \text{ K/T}$. These constants specific to LiHoF₄ are substituted in Eq. (16), and we obtain

$$H_{\text{eff}} = \frac{1}{2} \times 0.214 \sum_{i \neq j} L_{ij}^{zz} \sigma_i^z \sigma_j^z + \frac{1}{2} \times 0.214 \sum_{i, NN} J_{\text{ex}} \sigma_i^z \sigma_j^z - 4.635 B_{\text{eff}}^x \sum_i \sigma_i^x. \quad (17)$$

A comparison of Eqs. (16) and (17) immediately yields the crucial correspondence between the effective transverse magnetic field B_{eff}^x (expressed in T) and the physical transverse field B_x (also expressed in T):

$$B_{\text{eff}}^x = \frac{\Delta(B_x)}{2 \times 4.635 \times [\epsilon(B_x)]^2}. \quad (18)$$

We note that the dependence of B_{eff}^x on B_x in Fig. 2 is indeed quadratic for small values of B_x , as dictated by second-order perturbation theory, but the dependence becomes increasingly weaker as B_x increases. This demonstrates that in the quantum critical regime of large transverse fields and vanishing temperature, perturbation theory arguments are not adequate.

At this point, a subtlety in the definition of ‘‘temperature’’ needs to be mentioned. All our further calculations use H_{eff} as in Eq. (17), but the physical Hamiltonian is H_{Ising} , which modifies the energy scale by a factor $[\epsilon(B_x)]^2$ [see Eq. (15)]. In both mean-field theory and quantum Monte Carlo calculations, the temperature enters only in the definition of the Boltzmann weight of a configuration or a state vector in the form ($k_B=1$)

$$\rho = \exp\left(-\frac{H_{\text{Ising}}}{T}\right) = \exp\left(-\frac{[\epsilon(B_x)]^2 H_{\text{eff}}}{T}\right) = \exp\left(-\frac{H_{\text{eff}}}{T_{\text{eff}}}\right), \quad (19)$$

where the physical temperature T is related to the effective temperature T_{eff} by

$$T = [\epsilon(B_x)]^2 T_{\text{eff}}. \quad (20)$$

B. A possible three-state description of the effective Ising model

In this section, we digress from the discussion a bit to show that it is also possible to capture the degeneracy splitting $\Delta(B_x)$ using a simple three-state model of the system, but it leaves out the effect of the matrix elements of the ground state doublet with the higher-lying states. If we consider the states $|\alpha\rangle$, $|\beta\rangle$ and $|\gamma\rangle$ at $B_x=0$ as the basis states, then the crystal field Hamiltonian V_C is simply diagonal in this basis, and looks similar to

$$V_C = \begin{pmatrix} 0.0 & 0 & 0 \\ 0 & 0.0 & 0 \\ 0 & 0 & \Delta \end{pmatrix}, \quad (21)$$

where $\Delta=10.8 \text{ K}$.

The operator J^x has only two nonzero matrix elements restricted within the three states in the absence of a transverse field. By choosing the phase of the wave functions properly, it is possible to make both of them real. These matrix elements are

$$\langle \alpha | J^x | \gamma \rangle = \langle \beta | J^x | \gamma \rangle = \rho, \quad (22)$$

where $\rho=2.4$. Then the Hamiltonian in Eq. (6) can be written in the three-state basis as

$$H_T = \begin{pmatrix} 0 & 0 & -g_L \mu_B B_x \rho \\ 0 & 0 & -g_L \mu_B B_x \rho \\ -g_L \mu_B B_x \rho & -g_L \mu_B B_x \rho & \Delta \end{pmatrix}. \quad (23)$$

This Hamiltonian can be exactly diagonalized, and defining $\tilde{B}_x = g_L \mu_B B_x \rho$, the eigenvalues are

$$E_0 = \frac{\Delta}{2} - \frac{1}{2} \sqrt{\Delta^2 + 8\tilde{B}_x^2},$$

$$E_1 = 0,$$

$$E_2 = \frac{\Delta}{2} + \frac{1}{2} \sqrt{\Delta^2 + 8\tilde{B}_x^2}. \quad (24)$$

The eigenstates can be schematically written as

$$|\psi_0\rangle = \frac{1}{\sqrt{2}}(|\alpha\rangle + |\beta\rangle) + \varepsilon_0 |\gamma\rangle,$$

$$|\psi_1\rangle = \frac{1}{\sqrt{2}}(|\alpha\rangle - |\beta\rangle),$$

$$|\psi_2\rangle = |\gamma\rangle + \varepsilon_2(|\alpha\rangle + |\beta\rangle), \quad (25)$$

where the symbols ε_0 and ε_2 signify small admixtures.

It is readily seen that the transverse field splits the degeneracy by an amount $\Delta(B_x) = E_1 - E_0$. The gap is quadratic in B_x when $\tilde{B}_x \ll \Delta$, but it is, in fact, linear when $\tilde{B}_x \gg \Delta$. How-

ever, we see that the lowest excited state has an eigenvalue of zero for all B_x , unlike the real system, where it bends downwards with increasing B_x . Thus the three state model cannot capture the repulsion from the higher-lying states. Even then, it explicitly shows that the physics near the quantum critical point is ill-described by second-order perturbation theory.

C. Domains in LiHoF₄ and the mean-field solution

The magnetic dipole interaction is long range, falling off as $1/r^3$, where r is the distance between two spins. A dipole-coupled Ising ferromagnet is expected to be well explained by mean-field theory for $d \geq 3$. As we shall see, mean-field theory does capture the qualitative behavior in the phase diagram, but is not very reliable for making quantitative predictions.

Our starting point is Eq. (17). The individual spin- $\frac{1}{2}$ degrees of freedom sit on a tetragonal unit cell of dimensions $(a, a, c) = (1, 1, 2.077)$ in units of $a = 5.175 \text{ \AA}$. Each unit cell has four spins, at the positions we denote as $[(0, 0, 0), (0, a/2, c/4), (a/2, a/2, -c/2)$ and $(a/2, 0, -c/4)]$. All the positions in the unit cell are measured from the Bravais lattice vector denoted by $\vec{R} + (0, 0, 0)$.

The long-range nature and angular dependence of the dipole interaction create a complex model in which the actual shape and lattice of the sample influences the ground state. Spins that lie in the same ab plane want to antialign, while spins along the same c axis want to order ferromagnetically. This angular dependence tends to favor ferromagnetism in long thin samples, while it prohibits a ferromagnetic state in spherical samples. Luttinger and Tisza¹² found, for example, a ferromagnetic ground state for the face-centered lattice in the shape of a prolate spheroidal sample of axis ratio larger than 6. However, in experiments on LiHoF₄ spherical,² cubic,⁴ and rectangular¹ shapes have been used with no apparent dependence of the results on the shape of the sample.

The reason for this sample-shape independence lies in the domain structure of LiHoF₄. Experimentally, there is evidence^{13,14} that LiHoF₄ forms long needle-shaped domains, with the long direction being along the c axis. Theoretically, this agrees with the work of Griffiths,¹⁵ where a proof is given that the free energy of a dipolar system is independent of the shape of the sample in the absence of an externally applied field. Since this is an Ising system, the magnetization alternates in sign between adjacent domains, which minimizes the global energy stored in the macroscopic fields outside the sample. Thus it would be incorrect, in the context of mean-field theory, to assume that the magnetization is uniform over the entire sample, since in fact, it is only uniform over a single domain.

To incorporate the effect of domains, we assume that an imaginary sphere sits deep inside a single domain.¹⁶ A single spin at the center of this sphere now experiences an effective field from the orientation of the magnetic dipoles both inside and outside the sphere. In the ferromagnetically ordered state, the magnetization of the domain in question can be assumed to be uniform, denoted now by M^z . The magnetic field acting on the domain as a whole is the external field

B_{ext}^z , and the susceptibility χ of the domain can be found from the relation

$$M^z = \chi B_{\text{ext}}^z. \quad (26)$$

On the other hand, if we consider the small imaginary sphere deep inside the domain, the susceptibility χ_{sph} of the sphere can be found from the equation relating the magnetization inside the sphere (since the sphere is a part of the domain, the magnetization inside it is M^z) and the magnetic field acting on the sphere B_{sph}^z

$$M^z = \chi_{\text{sph}} B_{\text{sph}}^z. \quad (27)$$

Apart from the external field B_{ext}^z , a spin inside the spherical cavity also experiences two magnetic fields, one from the magnetic surface charge density at the surface of the sphere, and the other from the magnetic surface charge density at the surface of the long needle-shaped domain. There is no contribution from the spins in the bulk of the domain, since the magnetization is uniform, and only the surface charges contribute. Then the magnetic field B_{sph}^z can be related to these macroscopic fields¹⁷

$$B_{\text{sph}}^z = B_{\text{ext}}^z - \frac{8\pi}{3} M^z + 4\pi M^z. \quad (28)$$

The second term on the right-hand side of the equation above is the contribution from the spins at the surface of the sphere, while the third term is the contribution from the spins at the surface of the domain. By substituting Eq. (28) in Eqs. (26) and (27) leads to the following relation:

$$\chi = \frac{1}{\chi_{\text{sph}} - \frac{4\pi}{3}}. \quad (29)$$

Equation (29) above is the magnetic version of the Clausius-Mosotti relation,¹⁷ which relates the macroscopic electric susceptibility of a system with the microscopic molecular polarizability. In fact, it is in some ways easier to derive from the analogy with electric dipoles. In that case, the field produced by the charge density at the surface of the spherical cavity is $(4\pi/3)M^z$ while there is no contribution from the surface of the domain.

We emphasize that this relation is obtained from a single assumption that the spins *outside* the sphere are treated in mean-field fashion. The microscopic variable χ_{sph} can be calculated approximately, using mean-field theory, or exactly, using quantum Monte Carlo (QMC) simulations over a sphere. The next part of this section explores how the domain structure can be incorporated in the mean-field scenario, while the following section contains the results from QMC simulations.

At this point, a comment on the effect of the transverse magnetic field on the domain formation is necessary. From the mapping to the Ising model, it is seen that the contribution of the transverse dipole interaction, L_{ij}^{xx} is negligible compared to the longitudinal dipole interaction L_{ij}^{zz} . Therefore, we may assume that the transverse magnetic field polarizes the Ising spins along the x direction uniformly

throughout the sample. In other words, the x component of the magnetization M^x is unaware of the domain structure formation in LiHoF₄.

D. Mean-field theory

Let us now calculate the mean-field critical temperature for a long, needle-shaped domain. We therefore place the sphere deep inside a single domain. The mean-field critical temperature is given by the local field, which is given by the sum over all dipoles within the sphere. In the presence of domains, this field must be augmented by the field acting on the sphere B_{sph}^z .

With no domains a single spin at the center of the sphere therefore experiences an effective longitudinal mean-field given by

$$B_{\text{MF}}^z = \left(\sum_{j \neq 0}^{\text{sphere}} L_{0j}^{zz} \right) \times \left(\frac{m^z}{a^3} \right), \quad (30)$$

where m^z is the magnetic moment of a single dipole

$$m^z = \left(\frac{g_{\parallel} \mu_B}{2} \right) \langle \sigma^z \rangle. \quad (31)$$

The value of the lattice sum in Eq. (30) can be easily obtained by summing over larger and larger spheres, and the convergence is found to be very rapid. The value for LiHoF₄ is

$$\sum_{j \neq 0}^{\text{sphere}} L_{0j}^{zz} = 3.205. \quad (32)$$

In order to take the domain into account we combine Eqs. (28) and (30). Since the macroscopic magnetization is given by

$$M^z = N_0 m^z, \quad (33)$$

where N_0 is the number density of dipoles, we simply have to augment the value of the lattice sum in Eq. (32) by the value $(4\pi/3)N_0 a^3$. Since $N_0 = 4/aac$ and $c/a = 2.077$, it follows that $(4\pi/3)N_0 a^3 = 8.067$.

This leads to the value of the critical temperature at the classical limit.

$$T_C = 0.214 \text{ K} \times (3.205 + 8.067) \approx 2.41 \text{ K}. \quad (34)$$

On the other hand, the new critical effective field at the quantum limit is given by

$$B_{\text{eff},C}^x = \frac{2.41 \text{ K}}{4.635 \text{ K/T}} \approx 0.52 \text{ T}, \quad (35)$$

which corresponds to a physical critical transverse field of $B_{x,C} \approx 4.11 \text{ T}$.

We note that the critical temperature at the classical limit 2.41 K is 57% larger than the experimentally observed value of 1.53 K. This behavior is encouraging, in the sense that mean-field theory should always overestimate the ordered region. As far as the quantum limit is concerned, it may seem that the mean-field estimate is wrong, since 4.11 T is about

16% smaller than the experimentally observed value of 4.9 T. However, we have entirely neglected the on-site hyperfine interaction between the electronic cloud and the Ho nucleus. At low temperatures, this interaction affects the phase boundary significantly.² Therefore, at this point, we cannot yet compare our results for the quantum limit with experiment.

As a consistency check to our mean-field treatment of the domain structure, we perform the lattice sum directly over a long cylinder. The summation is done by considering a series of long cylinders with increasing base area. For each cylinder with a fixed base area, the length is increased until convergence is obtained. The series converges quite rapidly and as a final result we have

$$- \sum_{j \neq 0}^{\text{cylinder}} \left(\frac{\tilde{r}_j^2 - 3\tilde{z}_j^2}{\tilde{r}_j^5} \right) = 11.272 = 3.205 + 8.067, \quad (36)$$

in perfect agreement with the mean-field approach described above. We note that the mean-field theory calculation in Ref. 2 does not take into account the physics of domain formation but rather simply rescales the effective couplings to force a fit to the observed T_C and $B_{x,C}$.

V. QUANTUM MONTE CARLO SIMULATIONS ON LiHoF₄

We perform extensive QMC simulations of the dipole-coupled quantum Ising model, described by the Hamiltonian in Eq. (17). We use a recently introduced⁹ stochastic series expansion (SSE) cluster quantum Monte Carlo method for which computational time scales as $N \ln(N)$, where the number of spins is given by N . In traditional single-spin-flip simulations of long-range models the computational time typically scales as N^2 , due to the summation over interactions between all pairs of spins. The improved scaling enables us to increase the precision and reach large system sizes.

Our starting point is again Eq. (29), which relates a microscopic quantity χ_{sph} to a macroscopic quantity χ . From Eq. (29), we find that χ can diverge, even when B_{ext}^z vanishes, when

$$\chi_{\text{sph}} = \frac{3}{4\pi}. \quad (37)$$

We proceed to evaluate χ_{sph} exactly using QMC simulations as a function of T_{eff} and B_{eff}^x . At the point where the condition in Eq. (37) is met, χ , the macroscopic susceptibility, diverges and the system is critical.

Truncating the sum in the Hamiltonian at the boundary of the sphere and treating the dipoles outside the sphere in mean-field fashion can be considered a boundary condition in the Monte Carlo simulation. This so-called reaction-field method¹⁸ is not the only way to incorporate the long-range interaction in an efficient way. An alternative is to consider a large number of periodic images of the simulation volume. Performing the necessary sums over all dipoles in the simulation volume and the image volumes is very time consuming, but the sums can often be efficiently performed using the Ewald summation technique.¹⁹ In this work we have not attempted to compare the relative advantages of the methods,

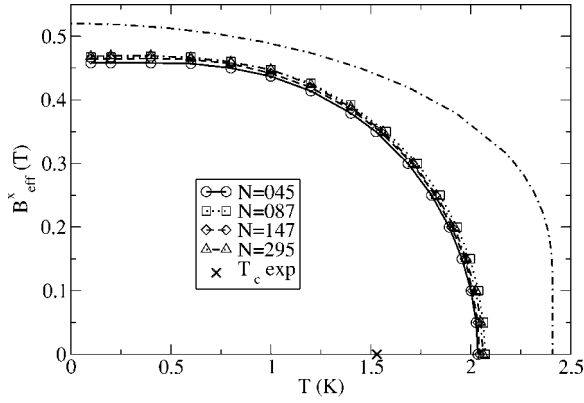


FIG. 3. The phase diagram as a function of effective temperature and effective magnetic field obtained from quantum Monte Carlo simulations on different lattice sizes. The upper curve is the mean-field solution.

but we have found the reaction-field method very convenient. An earlier comparison²⁰ found the Ewald summation method also quite reliable.

Operationally, the susceptibility χ_{sph} is defined as the spin-spin correlation function in imaginary time, averaged over all spins inside the sphere.

$$\chi_{\text{sph}} = \frac{\alpha}{N} \sum_{ij} \int_0^\beta d\tau \langle \sigma_i^z(\tau) \sigma_j^z(0) \rangle. \quad (38)$$

The prefactor α is given by

$$\alpha = N_0 \left(\frac{g_{\parallel} \mu_B}{2} \right)^2. \quad (39)$$

The imaginary time integral in Eq. (38) can be evaluated directly by the SSE method.²¹ The condition for criticality can be now be written as

$$\frac{1}{N} \sum_{ij} \int_0^\beta d\tau \langle \sigma_i^z(\tau) \sigma_j^z(0) \rangle = \frac{3}{4\pi N_0} \left(\frac{2}{g_{\parallel} \mu_B} \right)^2 = 0.579 \text{ K}^{-1}. \quad (40)$$

The simulation is done over a sequence of spheres with increasing radius. We find that the critical curve given by the above condition converges fairly quickly as the radius is increased. In the QMC calculation the fluctuations within the sphere are fully included, and we stress that although we use a mean-field result for the part of the domain exterior to the sphere, the final result has converged and should not, in any way, be considered a mean-field result. One could also argue that the field originating from dipoles in other domains may affect the critical temperature in LiHoF_4 . However, the material forms domains in order to minimize the energy density of the magnetic field, so this field should be very small. The same arguments hold also for the case of a transverse field, and the same condition is used in the presence of a transverse field. Figure 3 shows the phase diagram for the mean-field solution as well as for the Monte Carlo simulation.

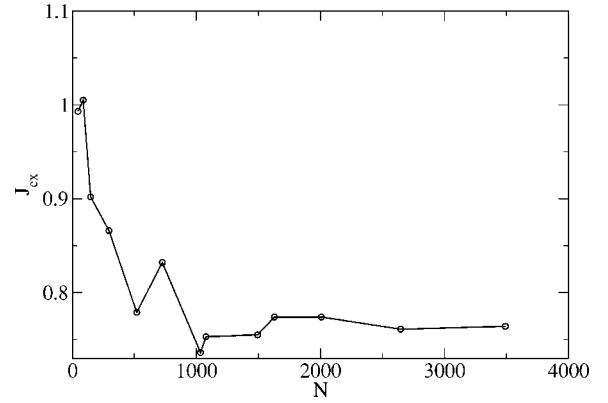


FIG. 4. Exchange energy needed to tune the critical temperature.

The results of Fig. 3 seem reasonable in the sense that the QMC solution yields a lower critical temperature than the mean-field solution. The mean-field solution is within 20% of the QMC solution, and it does therefore not suffice to describe the system at a more precise quantitative level, even for the present case of a long-range interaction in three dimensions. This is interesting since the upper critical dimension for a uniaxial dipolar interaction is expected to be 3, and the critical behavior should be described by mean-field theory with logarithmic corrections.^{22,23} The finite-size effects in Fig. 3 are quite small already for moderate system sizes and the result for the largest system size ($N=295$ dipoles) is $T_c=2.03$ K at $B_x=0$ and $(B_{\text{eff}}^x)_C=0.47$ T at the quantum limit. The critical temperature is still significantly above the experimental value of 1.53 K, but this discrepancy may be attributed to an additional exchange interaction, which we discuss shortly. The effective transverse field of 0.47 T corresponds to a physical transverse field of approximately 3.77 T. But, as stated earlier, comparison of the critical field with experimental value at the quantum limit is possible only when the hyperfine interaction is included in the model.

Exchange interaction. A major question at this point is why the critical temperature of the model is about half a K higher than the experimental value. One factor that lowers the critical temperature is the antiferromagnetic Heisenberg exchange interaction. Since there has been no direct observation of the strength of the interaction, we treat it as a free parameter J_{ex} as in Eq. (17). First we consider the mean-field solution with the domain structure. If we assume an exchange interaction of strength $J_{\text{ex}}=1.03$ the mean-field critical temperature is obtained as $T_c=0.2140\text{K} \times (11.271-4 \times 1.03)=1.53$ K, since every spin has four nearest neighbors.

Next we perform Monte Carlo simulations, where we tune the value of the exchange interaction to obtain a critical temperature of 1.53 K. This is done for a sequence of spheres with increasing radius, and the required exchange parameters are shown in Fig. 4. The corresponding phase diagram is shown in Fig. 5. There is still a strong (and nonmonotone) size dependence in the exchange parameter due to fluctuations in the number of surface bonds as the radius of the sphere increases, but the phase diagram shows very little size dependence. The exchange parameter itself has not con-

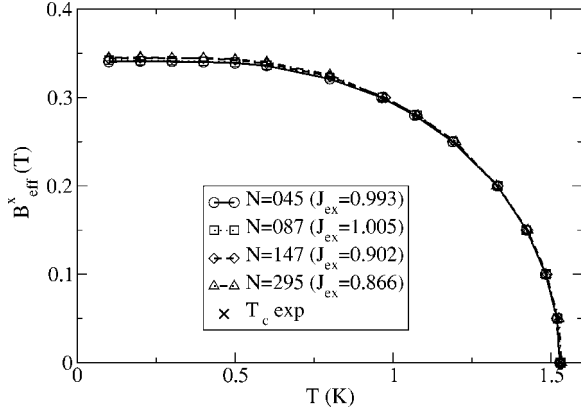


FIG. 5. Critical temperature as a function of effective transverse field, with an exchange interaction.

verged for the system sizes we study, but the results for the largest system sizes averages to about 0.75. This is about 25% smaller than the mean-field value, which seems reasonable. A value of $J_{\text{ex}}=0.75$ corresponds to an antiferromagnetic exchange interaction of strength 0.16 K between neighboring spins. This can be compared to the dipolar interaction between nearest neighbors, which is ferromagnetic and of strength 0.31 K, or about twice the exchange interaction. If we instead sum over all bonds connected to a given site in an ordered domain, the dipolar interaction is of strength $0.214 \times 11.271 \text{ K} = 2.4 \text{ K}$, while the exchange energy is of order $0.214 \times 4 \times 0.75 \text{ K} = 0.64 \text{ K}$. It is difficult to know if this is a reasonable value for the exchange, and a more stringent test comes when the whole phase diagram in can be compared to the experimental result. In the next section, we consider including the hyperfine interaction, which enables us to compare the phase diagram to experimental data.

The reason for the strong finite-size effect in the exchange parameter is that the exchange interaction for all broken bonds at the surface of the sphere is neglected in this calculation. If a spin is located close to the boundary of the sphere then one, two or three of its four nearest neighbors may be located outside the sphere. Even for the largest system size ($N=3491$) in Fig. 4, only 80% of the spins have all four nearest neighbors inside the sphere. The fraction of spins that have only one, two or three nearest neighbors inside the sphere fluctuates very rapidly as the size of the sphere is increased. However, this is a boundary effect and should disappear as the system size is increased further.

VI. THE HYPERFINE INTERACTION

The dynamics of LiHoF₄ at low temperatures is complicated by the hyperfine interaction between the electrons in the Ho³⁺ ion and the Ho nucleus.² This interaction is assumed to be on site, and its strength is characterized by the hyperfine constant A , which is equal to 0.039 K for LiHoF₄.^{24–26} At low temperatures, the hyperfine interaction prefers ordering and the final phase boundary is a result of the competition between the transverse field, which tries to destroy the ferromagnetic ordering, and the hyperfine interaction.

Consider the truncated Hamiltonian in Eq. (6). Since the value of the total nuclear angular momentum I in LiHoF₄ is $\frac{7}{2}$, the actual Hilbert space of the electron-nucleus system for a given site is, in reality, $17 \times 8 = 136$ dimensional. With the inclusion of the hyperfine coupling, the truncated Hamiltonian in Eq. (6) should be written as

$$H_{\text{hyp}} = [V_C(\vec{J}) - g_L \mu_B B_x J^x] \otimes 1_N + A \sum_{\mu=x,y,z} J^\mu \otimes I^\mu, \quad (41)$$

where 1_N is the eight-dimensional unit matrix in the nuclear sector of the Hilbert space.

The Hamiltonian in Eq. (41) is a 136-dimensional matrix, and in the absence of the hyper-fine interaction, each electronic crystal-field wave function is eightfold degenerate. The hyperfine interaction breaks this degeneracy to the order of the strength of A . We adopt the viewpoint that the transverse magnetic field is renormalized because of the hyperfine interaction, in a fashion controlled by the temperature. This renormalization can be extracted by matching the longitudinal susceptibility of a single Ho³⁺ ion without the presence of the hyperfine interaction as described below.

The susceptibility χ_{zz} for a single ion is easy to define in the 136-dimensional Hilbert space. We diagonalize the Hamiltonian in Eq. (41) with $A=0$ and $A=0.039 \text{ K}$. Let the eigenstates in the 136-dimensional Hilbert space be denoted by $|\psi_m^0\rangle$ when $A=0$ and $|\psi_m^1\rangle$ when A is nonzero, and the corresponding energy eigenvalues as E_m^0 and E_m^1 , $m=1, \dots, 136$ in both cases. For a temperature $T=1/\beta$, the longitudinal susceptibility can be defined as

$$\chi_{zz}^i = \frac{\beta}{Z_{i,m,n=1,\dots,136}} \sum_{i'} |\langle \psi_m^i | J^z \otimes 1_N | \psi_n^i \rangle|^2 \times e^{-\beta E_m^i} \frac{2}{Z_{i,m,n=1,\dots,136}} \sum_{i''} \frac{|\langle \psi_m^i | J^z \otimes 1_N | \psi_n^i \rangle|^2 e^{-\beta E_m^i}}{E_m^i - E_n^i}, \quad (42)$$

where $i=0,1$. The primed sum is over states degenerate in energy, while the double-primed sum is over states nondegenerate in energy. Figure 6 shows how the susceptibilities at the typical temperature $T=0.444 \text{ K}$ differ for a range of values of the transverse field depending on whether the hyperfine interaction is turned on or not.

From the plot of the susceptibilities, it is clear that the hyperfine interaction renormalizes the magnetic field. This effect is temperature dependent, and the shift in susceptibility decreases as the temperature is increased. For instance, the Ising mapping and quantum Monte Carlo simulations yield a typical point on the phase boundary as $(T_C, B_{x,C}) = (0.444 \text{ K}, 2.949 \text{ T})$. In Fig. 6 we see that $\chi_e^{zz}(A=0, T=0.444 \text{ K}, B_x=2.949 \text{ T})$ equals $\chi_e^{zz}(A=0.039 \text{ K}, T=0.444 \text{ K}, B_x=3.282 \text{ T})$. Thus, we conclude that the critical transverse field of 2.949 T is renormalized to the critical transverse field of 3.282 T in the presence of the hyperfine interaction. This simple renormalization program can be carried out for all the points on the quantum Monte Carlo phase

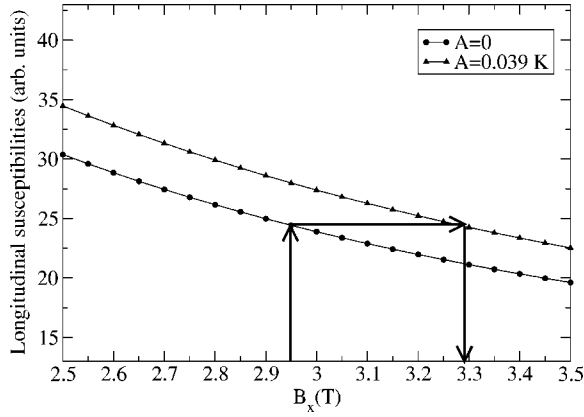


FIG. 6. Comparison of the single-ion longitudinal susceptibilities with and without the hyperfine interaction. We make the approximation of assuming that the increase in longitudinal susceptibility caused by the nuclei can be modeled by simply renormalizing the transverse field downwards by the appropriate amount.

boundary. This procedure yields a phase diagram that shows how the hyperfine interaction affects the phase boundary significantly in the quantum regime.

A. Magnetic phase diagram from quantum Monte Carlo and hyperfine interaction

Figure 7 shows a comparison of the theoretically obtained phase diagram with the experimental phase diagram obtained through susceptibility experiments.² We get a quantum critical point of $B_{x,C}=4.66$ T, which is approximately 6% smaller than the experimental value. However, serious deviations also occur at temperatures higher than $T \sim 1$ K, where the effect of the nuclear interaction is negligible. This leads us to conclude that the deviation really stems from the mapping to the Ising model. The Ising model mapping is strongly determined by the strength of the degeneracy splitting in the ground-state doublet as the transverse magnetic field is turned on, which in turn strongly depends upon the values of the crystal-field parameters. In a subsequent section, the uncertainties in the crystal-field parameters and their effect on the physics are discussed.

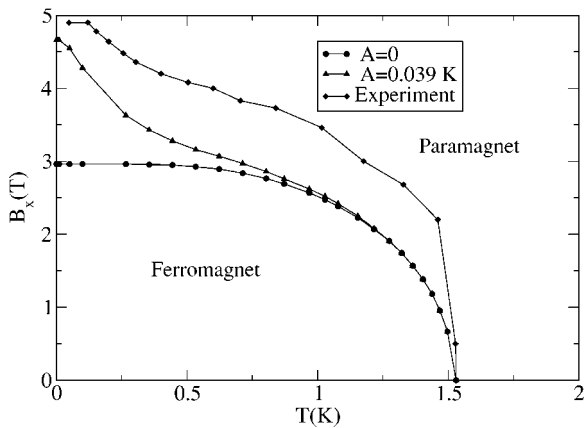


FIG. 7. The complete phase diagram of LiHoF₄. Experimental data is from Ref. 2.

B. Hyperfine interaction and the Ising model

The actual computation of the longitudinal susceptibility of the ion-nucleus system in the presence of a hyperfine interaction requires the knowledge of all the eigenstates of the 136-dimensional Hilbert space. However, the physics of why the hyperfine interaction enhances the longitudinal susceptibility can be understood by considering a toy system consisting of a single spin- $\frac{1}{2}$ electron coupled to a spin- $\frac{1}{2}$ nucleus through a hyperfine interaction. It shall be seen that the enhancement of susceptibility is really a subtle effect captured in second-order perturbation theory.

Let us consider a single spin- $\frac{1}{2}$ electron placed in a transverse magnetic field h_x (we assume that the nucleus does not couple to the magnetic field: this is a reasonable assumption since the nuclear g factor in LiHoF₄ is approximately 1000 times smaller than the electronic Landé g factor). Then the Hamiltonian is

$$H = -h_x \sigma_e^x \otimes 1_N. \quad (43)$$

The subscripts e and N refer to the electronic and nuclear degrees of freedom, respectively. The Hilbert space is $[(2 \times \frac{1}{2} + 1)(2 \times \frac{1}{2} + 1) = 4]$ dimensional, and the transverse field splits the Hilbert space in two multiplets, each of which is twofold degenerate. The ground electronic multiplet consists of the states $|\rightarrow\rangle_e \otimes |\uparrow\rangle_N$ and $|\rightarrow\rangle_e \otimes |\downarrow\rangle_N$, while the excited electronic multiplet consists of the states $|\leftarrow\rangle_e \otimes |\uparrow\rangle_N$ and $|\leftarrow\rangle_e \otimes |\downarrow\rangle_N$, the difference in energy between the two multiplets being $2h_x$. The longitudinal susceptibility can be easily evaluated using the expression in Eq. (42) (with suitable modifications for the toy system), and we find

$$\chi_{zz} = \frac{1}{h_x} \quad (44)$$

at $T=0$.

If the hyperfine interaction is turned on, the degeneracies between the states in the nuclear sector is lifted in each multiplet, and this changes the susceptibilities. Let the perturbing hyperfine interaction be written as

$$V_{\text{hyp}} = A_{\parallel} \sigma_e^z \sigma_N^z + A_{\perp} \sigma_e^x \sigma_N^x. \quad (45)$$

Even though the hyperfine strengths are isotropic in the physical system, introducing anisotropy helps us to understand the roles played by the longitudinal and transverse components of the hyperfine interaction transparently. The special case of isotropy, $A_{\parallel}=A_{\perp}$, will be considered at the end.

In first order degenerate perturbation theory, the electronic states are all polarized in the x direction, and only A_{\perp} has any nonzero matrix element within the same degenerate electronic multiplet. Thus A_{\parallel} drops out of the physics in first-order perturbation theory.

In Fig. 8, the states in the four-dimensional Hilbert space are $|\psi_1^0\rangle = |\rightarrow\rangle_e \otimes |\leftarrow\rangle_N$, $|\psi_2^0\rangle = |\rightarrow\rangle_e \otimes |\rightarrow\rangle_N$, $|\psi_3^0\rangle = |\leftarrow\rangle_e \otimes |\rightarrow\rangle_N$, and $|\psi_4^0\rangle = |\leftarrow\rangle_e \otimes |\leftarrow\rangle_N$. The zero temperature susceptibility is now given by

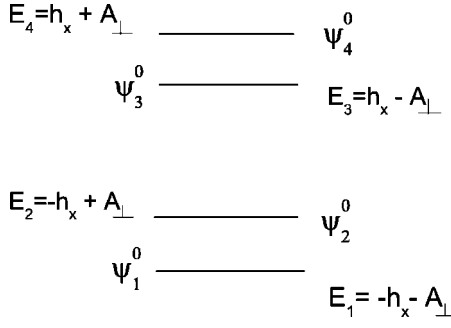


FIG. 8. Ion energy spectrum (for a spin-1/2 nucleus) with the hyperfine interaction treated in first order perturbation theory.

$$\chi_{zz} = \frac{1}{h_x + |A_\perp|}. \quad (46)$$

Thus it is obvious that the longitudinal susceptibility always decreases in first-order perturbation theory. The transverse component of the hyperfine interaction always acts as an extra transverse field, which implies that the hyperfine interaction should lower the critical field, at least in first-order perturbation theory.

However, if we consider second-order perturbation theory, we can show that, when the hyperfine interaction is *isotropic*, the net effect is actually an increase in the longitudinal susceptibility at $T=0$. In second order, only A_\parallel contributes to further splitting of the energy spectrum. More importantly, the ground state $|\rightarrow\rangle_e \otimes |\leftarrow\rangle_N$ is mixed with the state $|\leftarrow\rangle_e \otimes |\rightarrow\rangle_N$, and the state $|\rightarrow\rangle_e \otimes |\rightarrow\rangle_N$ is mixed with the state $|\leftarrow\rangle_e \otimes |\leftarrow\rangle_N$ both with an amplitude given by $\varepsilon = A_\parallel/h_x$. Thus, up to second-order perturbation theory we have the following spectrum:

$$\begin{aligned} |\psi_1\rangle &= |\psi_1^0\rangle - \frac{A_\parallel}{h_x} |\psi_3^0\rangle, \\ |\psi_2\rangle &= |\psi_2^0\rangle - \frac{A_\parallel}{h_x} |\psi_4^0\rangle, \\ |\psi_3\rangle &= |\psi_3^0\rangle + \frac{A_\parallel}{h_x} |\psi_1^0\rangle, \\ |\psi_4\rangle &= |\psi_4^0\rangle + \frac{A_\parallel}{h_x} |\psi_2^0\rangle. \end{aligned} \quad (47)$$

The energies of the states up to second-order in perturbation theory are given by

$$\begin{aligned} E_1 &= -h_x - A_\perp - \frac{A_\parallel^2}{2h_x}, \\ E_2 &= -h_x + A_\perp - \frac{A_\parallel^2}{2h_x}, \\ E_3 &= +h_x - A_\perp + \frac{A_\parallel^2}{2h_x}, \end{aligned}$$

$$E_4 = +h_x + A_\perp + \frac{A_\parallel^2}{2h_x}. \quad (48)$$

This gives rise to a nonzero matrix element of σ_e^z between $|\psi_1\rangle$ and $|\psi_2\rangle$, and this term serves to cancel the decrease in susceptibility because of first-order contribution from A_\perp . The exact expression for the longitudinal susceptibility at $T=0$ is given by

$$\chi_{zz} = \frac{\left[1 - \left(\frac{A_\parallel}{2h_x}\right)^2\right]^2}{h_x + A_\perp + \frac{A_\parallel^2}{2h_x}} + \frac{A_\parallel^2}{2h_x A_\perp}. \quad (49)$$

The denominator in the first term in the right-hand side of Eq. (49) can be easily expanded in terms of the ratios A_\perp/h_x and $A_\parallel^2/2h_x^2$, and the susceptibility expression turns out to be ($h_x \gg A_\parallel, A_\perp$)

$$\chi_{zz} = \frac{1}{h_x} + \left(\frac{A_\parallel^2}{A_\perp} - A_\perp\right) \frac{1}{h_x^2} + O\left(\frac{1}{h_x^3}\right) + \dots \quad (50)$$

The crux of the increase in susceptibility lies in the fact that the term proportional to $1/h_x^2$ is positive when $A_\parallel \geq A_\perp$. The increase in susceptibility is not a generic feature of the *ion-nuclear* interaction for all values of A_\parallel and A_\perp , but is present when the interaction is isotropic, as in LiHoF₄. The transverse component always drives the susceptibility lower, but the longitudinal component can compete and win for a certain range of values, and the change in susceptibility is quadratic in A_\parallel . We emphasize that this positive contribution arises from the nonzero matrix element between two states that were degenerate in the absence of the hyperfine interaction.

This schematic problem of a spin- $\frac{1}{2}$ electron coupled to a spin- $\frac{1}{2}$ nucleus through a hyper-fine interaction serves nicely to illustrate the physics behind an increase in the longitudinal susceptibility of the electrons due to the hyperfine interaction. In LiHoF₄, every electronic state is split into eight nuclear states when the hyperfine interaction is turned on. There is no matrix element of J_z within the same electronic multiplet when $A_\parallel=0$. When $A_\parallel \neq 0$, a nonzero matrix element of J_z develops between two lowest nuclear states in the ground electronic multiplet, the square of the matrix element varying quadratically as A_\parallel . Exactly as outlined in the schematic problem, this matrix element causes an increase in the longitudinal susceptibility of the electron.

C. Projecting the hyperfine interaction

The hyperfine interaction involves the electronic angular momentum J^μ . Following the mapping to the Ising subspace in the previous sections, we can map these degrees of freedom to effective Ising degrees of freedom. This gives rise to a hyperfine interaction term that operates in an effectively $16(=2 \times 8)$ -dimensional Hilbert space. However, this gives rise to a hyperfine interaction whose strength depends on the magnetic field. Using the mapping in Eq. (7), Eq. (8) and the hyperfine interaction in Eq. (41), the effective single-site Hamiltonian now becomes

$$H = -\frac{\Delta(B_x)}{2}\sigma_e^x \otimes 1_N + AC_{\alpha\beta}(B_x)\sigma^\alpha \otimes I^\beta. \quad (51)$$

Using the projected Hamiltonian in Eq. (51), we can naturally understand why the longitudinal component of the hyperfine interaction wins over the transverse one. The longitudinal component is proportional to $C_{zz}(B_x)$, which is significantly larger than all the other components at the magnetic field regime of interest. The analysis of the previous section remains valid in a 16-dimensional Hilbert space, and the susceptibility is always enhanced due to the contribution from the longitudinal component of the hyperfine interaction $A_{\parallel} = AC_{zz}(B_x)$.

D. Uncertainties in the crystal-field parameters

The quantitative details of the LiHoF₄ depend sensitively on the values of the various crystal-field parameters (CFP) used in constructing the crystal field Hamiltonian (please see the Appendix for details). For example, we have found that the value of the critical transverse field $B_{x,C}$ varies by as large as 25% when the CFP B_2^0 is varied by 10%. However, the parameters cannot be determined directly by experiments, but are used as fitting parameters to fit theoretical calculations to experimental data. There have been attempts to determine the CFP's by fitting to spectroscopic data¹⁰ or to susceptibility measurements.¹¹ However, we have found that the results of theoretical calculations become more and more sensitive to the values of CFP's as the transverse field is increased. As we have shown in earlier sections, the most important physical quantity that determines the phase diagram is the splitting between the two lowest states $\Delta(B_x)$, that smoothly and monotonically increases with the transverse field. Thus we propose a spectroscopic experiment in the presence of a transverse field to determine $\Delta(B_x)$. However, the quantum regime of the phase diagram is complicated due to the presence of hyperfine interaction. The effect of the hyperfine interaction is also extremely sensitive to the values of the CFP's, and this effect is very difficult to calculate theoretically. Thus we propose the experiment be carried out in a regime of the phase diagram where the quantum fluctuations due to the hyperfine interaction are negligible, but the fluctuations caused by the transverse magnetic field are still significant. Thus we propose an experiment to determine $\Delta(B_x)$ in the magnetic field range 2.0–3.0 T. In this regime, our theoretical calculations show that the splitting energy varies between ~ 1.6 –3.0 K. This corresponds to a microwave frequency range of ~ 20 –70 GHz. A spectroscopic experiment that determines $\Delta(B_x)$ accurately is the most important ingredient needed to determine the phase diagram accurately. Even though a single spectroscopic experiment is not enough to determine the values of all the crystal field parameters uniquely, we have found that the only other important parameter in the effective Ising Hamiltonian $C_{zz}(B_x)$ is extremely robust even to large changes in the crystal field parameters. Thus, an accurate determination of $\Delta(B_x)$ is enough to compute the phase diagram from the effective Ising model.

VII. SUMMARY AND CONCLUSIONS

It has been postulated that LiHoF₄ is an example of an Ising-like system, and when the sample is placed in a magnetic field transverse to the Ising direction, it is an example of a quantum Ising system with magnetic dipole interaction being the ordering interaction. However, the quantum Ising model, Eq. (1), has never been used to obtain physical results for the system. We derive the physical Ising model by a nonperturbative mapping to the Hilbert space spanned by the ground-state doublet. We then do a quantum Monte Carlo simulation to obtain the phase diagram, also incorporating the domain structure in the process. This is a step beyond mean-field theory and the calculation is sufficiently accurate that uncertainty in the predicted phase diagram is now limited by uncertainties in the crystal-field parameters. As a spin off, we are able to compute the phenomenological exchange interaction parameter that modifies the phase diagram considerably in the classical regime. The hyperfine interaction poses considerable problems in comparing the phase diagram obtained from the quantum Monte Carlo simulations to the experimental data. We have made the approximation that the effects of the hyperfine interaction can be completely recovered through a renormalization of the magnetic field.

LiHoF₄ is a material in which the magnetic quantum and classical phase transitions can be controlled with great precision. Neutron scattering studies have been done on LiHoF₄ to obtain the spin-wave excitations in the system. By randomly replacing the magnetic Ho³⁺ with nonmagnetic Y³⁺ ions, spin-glass behavior has been observed. We believe that the existence of an Ising model that faithfully reproduces the physics in both the classical and the quantum regimes, will facilitate the investigations of the interesting properties of LiHoF₄ considerably.

ACKNOWLEDGMENTS

We thank Jens Jensen for many helpful discussions and for supplying us with a copy of Ref. 6. We also thank M. J. P. Gingras for many helpful discussions. P.H. acknowledges support by the Swedish Research Council and the Göran Gustafsson foundation. S.M.G. and P.B.C. were supported by Grant No. NSF DMR-0342157. A.W.S. was supported by the Academy of Finland, Project No. 26175.

APPENDIX: THE CRYSTAL-FIELD HAMILTONIAN

In LiHoF₄, the Ho³⁺ ions have an unfilled shell $4f$ with 10 electrons. The Hund's rules dictate that the ground configuration of a single Ho³⁺ ion should be $^5I_8(S=2, L=6, J=8)$. If there were no interactions with the neighboring ions, the ground state of a single ion will be 17-fold degenerate. However, the Coulomb interactions with the neighboring ions gives rise to an electric field that lifts this degeneracy. In general, this electric field depends strongly on the spatial symmetry of the crystals. In the simplest scenario, each ion is regarded as a point charge, and the spatial overlap of the wave function of an ion with its neighboring ion is neglected. This is the point-charge model for calculating crystal fields. The derivation of the crystal-field electrostatic potential takes

into account the lattice symmetry, and is most simply expressed in terms of operators called “operator equivalents.” We shall not discuss the details of the derivation here, but instead refer the reader to the article by Hutchings,²⁷ and references therein.

The operator equivalents are operators built out of the \vec{J} operators that act on the $(2J+1)$ -dimensional space determined by the value of J . However, they act only on the angular part of the wave function of the coupled system, and the matrix elements of the radial part of the wave function are usually incorporated as fitting parameters.

The number of operators needed to completely determine the crystal field Hamiltonian V_C , and the rules for deriving them, depend on the symmetry of the crystal and the ground-state configuration of the ion. These rules are clearly explained by Stevens²⁸ and Stevens and Bleaney.²⁹ Here we shall just list the operators that have nonzero matrix elements in the configuration 5I_8 of the Ho³⁺ ion in LiHoF₄.

In case of LiHoF₄, the relevant crystal field operators are

$$O_2^0 = 3J_z^2 - J(J+1),$$

$$O_4^0 = 35J_z^4 - 30J(J+1)J_z^2 + 25J_z^2 - 6J(J+1) + 3J^2(J+1)^2,$$

$$O_4^4(C) = \frac{1}{2}(J_+^4 + J_-^4),$$

$$O_6^0 = 231J_z^6 - 315J(J+1)J_z^4 + 735J_z^4 + 105J^2(J+1)^2J_z^2 - 525J(J+1)J_z^2 + 294J_z^2 - 5J^3(J+1)^3 + 40J^2(J+1)^2 - 60J(J+1),$$

$$O_6^4(C) = \frac{1}{4}(J_+^4 + J_-^4)[11J_z^2 - J(J+1) - 38] + \text{H. c.},$$

$$O_6^4(S) = \frac{1}{4i}(J_+^4 - J_-^4)[11J_z^2 - J(J+1) - 38] + \text{H. c.},$$

(A1)

where $J_+ = J_x + iJ_y$ and $J_- = J_x - iJ_y$.

Using these operators, the crystal-field Hamiltonian V_C can be written as

$$V_C = B_2^0 O_2^0 + B_4^0 O_4^0 + B_6^0 O_6^0 + B_4^4(C) O_4^4(C) + B_6^4(C) O_6^4(C) + B_6^4(S) O_6^4(S). \quad (\text{A2})$$

The radial matrix elements of the crystal field is extremely difficult to compute accurately even in a point-charge model. They are, therefore, incorporated within the constants B_l^m , known as crystal-field parameters (CFP's). The CFP's are generally used as fitting parameters. In LiHoF₄, for example, they are used to fit the crystal-field spectrum to observed spectroscopic data,^{10,25,30,31} and to susceptibility measurements.¹¹

In all our calculations, we use the CFP's proposed by Rønnow *et al.*⁶ Their values (in K) are listed below:

$$B_2^0 = -0.696,$$

$$B_4^0 = 4.06 \times 10^{-3},$$

$$B_6^0 = 4.64 \times 10^{-6},$$

$$B_4^4(C) = 0.0418,$$

$$B_6^4(C) = 8.12 \times 10^{-4},$$

$$B_6^4(S) = 1.137 \times 10^{-4}. \quad (\text{A3})$$

These values of CFP's were obtained⁶ by fitting the results of RPA spin-wave dynamics calculations to observed neutron scattering data, as well as to the two lowest energy levels of the crystal-field spectrum, as observed in spectroscopic measurements.³² However, there are no estimates of the accuracies to which these parameters are known. There was an earlier attempt to determine the CFP's by fitting to susceptibility data,¹¹ but there were very large error bars. Another attempt was made to determine the CFP's by fitting to spectroscopic measurements,¹⁰ but an incorrect symmetry (D_{2d}) of the crystal was used in the theoretical calculations, instead of the correct one S_4 .

¹W. Wu, B. Ellman, T. Rosenbaum, G. Aeppli, and D. H. Reich, Phys. Rev. Lett. **67**, 2076 (1991).

²D. Bitko, T. Rosenbaum, and G. Aeppli, Phys. Rev. Lett. **77**, 940 (1996).

³J. Brooke, D. Bitko, T. F. Rosenbaum, and G. Aeppli, Science **284**, 779 (1999).

⁴D. H. Reich, B. Ellman, J. Yang, T. Rosenbaum, G. Aeppli, and D. P. Belanger, Phys. Rev. B **42**, 4631 (1990).

⁵S. Ghosh, R. Parthasarathy, T. F. Rosenbaum, and G. Aeppli, Science **296**, 2195 (2002).

⁶H. M. Rønnow, R. Parthasarathy, G. Aeppli, and J. Jensen (unpublished).

⁷S.J.K. Jensen and K. Kjaer, J. Phys.: Condens. Matter **1**, 2361

(1989).

⁸H. Xu, B. Bergersen, and Z. Racz, J. Phys.: Condens. Matter **4**, 2035 (1992).

⁹A. W. Sandvik, Phys. Rev. E **68**, 056701 (2003).

¹⁰H. P. Christensen, Phys. Rev. B **19**, 6564 (1979).

¹¹P. E. Hansen, T. Johansson, and R. Nevald, Phys. Rev. B **12**, 5315 (1975).

¹²J. M. Luttinger and L. Tisza, Phys. Rev. **70**, 954 (1946).

¹³A. H. Cooke, D. A. Jones, J. F. A. Silva, and M. R. Wells, J. Phys. C **8**, 4083 (1975).

¹⁴J. E. Battison, A. Kasten, M. J.M. Leask, J. B. Lowry, and B. M. Wanklyn, J. Phys. C **8**, 4089 (1975).

¹⁵R. Griffiths, Phys. Rev. **176**, 655 (1968).

- ¹⁶H. Kjønsgberg and S. M. Girvin, in *Fundamental Physics of Ferroelectrics 2000: Aspen Center for Physics Winter Workshop*, edited by R. E. Cohen, AIP Conf. Proc. No. 535 (AIP, Melville, NY, 2000), p. 323.
- ¹⁷J. D. Jackson, *Classical Electrodynamics* (Wiley, New York, 1975).
- ¹⁸J. A. Barker and R. O. Watts, *Mol. Phys.* **26**, 789 (1973).
- ¹⁹P. P. Ewald, *Ann. Phys. (Leipzig)* **64**, 253 (1921).
- ²⁰R. Kretschmer and K. Binder, *Z. Phys. B* **34**, 375 (1979).
- ²¹A. W. Sandvik and J. Kurkijärvi, *Phys. Rev. B* **43**, 5950 (1991).
- ²²A. I. Larkin and D. E. Khmel'nitskii, *Sov. Phys. JETP* **29**, 1123 (1969).
- ²³A. Aharony, *Phys. Rev. B* **8**, 3363 (1973).
- ²⁴G. Mennenga, L. J. deJongh, and W. J. Huiskamp, *J. Magn. Mater.* **44**, 59 (1984).
- ²⁵J. Magarino, J. Tuchendler, P. Beauvillain, and I. Laursen, *Phys. Rev. B* **21**, 18 (1980).
- ²⁶R. Giraud, W. Wernsdorfer, A. M. Tkachuk, D. Mailly, and B. Barbara, *Phys. Rev. Lett.* **87**, 057203 (2001).
- ²⁷M. T. Hutchings, *Solid State Phys.* **16**, 227 (1964).
- ²⁸K. W. H. Stevens, *Proc. Phys. Soc., London, Sect. A* **65**, 209 (1952).
- ²⁹B. Bleany and K. W. H. Stevens, *Rep. Prog. Phys.* **16**, 108 (1953).
- ³⁰S. Salaun, M. Fornoni, A. Bulou, M. Rousseau, P. Simon, and J. Y. Gesland, *J. Phys.: Condens. Matter* **9**, 6941 (1997).
- ³¹N. I. Agladze, M. N. Popova, M. A. Koreiba, B. Z. Malkin, and V. R. Pekurovskii, *Zh. Eksp. Teor. Fiz.* **104**, 4171 (1993).
- ³²S. N. Gifeisman, A. M. Tkachuk, and V. V. Prizmak, *Opt. Spectrosc. (USSR)* **44**, 68 (1978).